Research Article | Vol. 25, No. 19 | 18 Sep 2017 | OPTICS EXPRESS 23334
Optics EXPRESS

Large area nanoimprint enables ultra-precise x-ray diffraction gratings

D. L. VORONOV,* E. M. GULLIKSON, AND H. A. PADMORE

Lawrence Berkeley National Laboratory, 1 Cyclotron Road, Berkeley, CA 94720
**dlvoronov@lbl.gov*

Abstract: A process for fabrication of ultra-precise diffraction gratings for high resolution x-ray spectroscopy was developed. A grating pattern with constant or variable line spacing (VLS) is recorded on a quartz plate by use of e-beam lithography with nanometer scale accuracy of the groove placement. The pattern is transferred to a massive grating blank by large area nanoimprint followed by dry or/and wet etching for groove shaping. High fidelity of the nanoimprint transfer step was confirmed by differential wavefront measurements. Successful implementation of the suggested fabrication approach was demonstrated by fabrication of a lamellar 900 lines/mm VLS grating for a soft x-ray fluorescence spectrometer.

OCIS codes: (050.1950) Diffraction gratings; (340.7480) X-rays, soft x-rays, extreme ultraviolet (EUV).

References and links

1. M. C. Hettrick and J. H. Underwood, "Varied space grazing incidence gratings in high resolution scanning spectrometers," AIP Conf. Proc. **147**, 237–245 (1986).
2. R. Reininger, K. Kriesel, S. L. Hulbert, C. Sánchez-Hanke, and D. A. Arena, "A soft x-ray beamline capable of canceling the performance impairment due to power absorbed on its optical elements," Rev. Sci. Instrum. **79**(3), 033108 (2008).
3. T. Warwick, Y.-D. Chuang, D. L. Voronov, and H. A. Padmore, "A Multiplexed High-Resolution Imaging Spectrometer for Resonant Inelastic Soft X-ray Scattering Spectroscopy," J. Synchrotron Radiat. **21**(4), 736–743 (2014).
4. J. Dvorak, I. Jarrige, V. Bisogni, S. Coburn, and W. Leonhardt, "Towards 10 meV resolution: The design of an ultrahigh resolution soft X-ray RIXS spectrometer," Rev. Sci. Instrum. **87**(11), 115109 (2016).
5. F. Senf, F. Bijkerk, F. Eggenstein, G. Gwalt, Q. Huang, R. Kruijs, O. Kutz, S. Lemke, E. Louis, M. Mertin, I. Packe, I. Rudolph, F. Schäfers, F. Siewert, A. Sokolov, J. M. Sturm, Ch. Waberski, Z. Wang, J. Wolf, T. Zeschke, and A. Erko, "Highly efficient blazed grating with multilayer coating for tender X-ray energies," Opt. Express **24**(12), 13220–13230 (2016).
6. http://www.inprentus.com/
7. http://www.shimadzu.com/opt/products/dif/o-k25cur0000006z3f.html
8. http://www.horiba.com/scientific/products/diffraction-gratings/for-scientific-applications/vacuum-uv-and-soft-x-ray-applications/
9. T. Namioka and M. Koike, "Aspheric wave-front recording optics for holographic gratings," Appl. Opt. **34**(13), 2180–2186 (1995).
10. http://www.helmholtz-berlin.de/forschung/oe/fg/nanometeroptik/technologiezentrum-optische-praezisionsgitter/historie-und-aktueller-stand-der-gitterentwicklung_en.html
11. http://www.esrf.eu/ID32
12. D. L. Voronov, E. M. Gullikson, F. Salmassi, T. Warwick, and H. A. Padmore, "Enhancement of diffraction efficiency via higher-order operation of a multilayer blazed grating," Opt. Lett. **39**(11), 3157–3160 (2014).
13. D. L. Voronov, E. H. Anderson, R. Cambie, S. Cabrini, S. D. Dhuey, L. I. Goray, E. M. Gullikson, F. Salmassi, T. Warwick, V. V. Yashchuk, and H. A. Padmore, "A 10,000 groove/mm multilayer coated grating for EUV spectroscopy," Opt. Express **19**(7), 6320–6325 (2011).
14. D. L. Voronov, P. Lum, P. Naulleau, E. M. Gullikson, A. V. Fedorov, and H. A. Padmore, "X-ray diffraction gratings: precise control of ultra-low blaze angle via anisotropic wet etching," Appl. Phys. Lett. **109**(4), 043112 (2016).
15. D. L. Voronov, P. Gawlitza, R. Cambie, S. Dhuey, E. M. Gullikson, T. Warwick, S. Braun, V. V. Yashchuk, and H. A. Padmore, "Conformal growth of Mo/Si multilayers on grating substrates using collimated ion beam sputtering," J. Appl. Phys. **111**(9), 093521 (2012).
16. D. L. Voronov, L. I. Goray, T. Warwick, V. V. Yashchuk, and H. A. Padmore, "High-order multilayer coated blazed gratings for high resolution soft x-ray spectroscopy," Opt. Express **23**(4), 4771–4790 (2015).
17. H. Gao, H. Tan, W. Zhang, K. Morton, and S. Y. Chou, "Air cushion press for excellent uniformity, high yield, and fast nanoimprint across a 100 mm field," Nano Lett. **6**(11), 2438–2441 (2006).

#303317 https://doi.org/10.1364/OE.25.023334
Journal © 2017 Received 26 Jul 2017; revised 1 Sep 2017; accepted 5 Sep 2017; published 14 Sep 2017

Optics EXPRESS

18. http://www.microresist.de/en
19. http://foundry.lbl.gov/facilities/nanofabrication/expertise.html
20. D. L. Voronov, S. Diez, P. Lum, S. A. Hidalgo, T. Warwick, N. Artemiev, and H. A. Padmore, "Fabrication of x-ray gratings by direct write mask-less lithography," Proc. SPIE **8848**, 88480Q (2013).
21. S. Gleason, J. Manton, J. Sheung, T. Byrum, C. Jensen, L. Jiang, J. Dvorak, I. Jarrige, K. Kaznatcheev, and P. Abbamonte, "Intrinsic resolving power of XUV diffraction gratings measured with Fizeau interferometry," Proc. SPIE (to be published).
22. T. Kimura, H. Ohashi, H. Mimura, D. Yamakawa, H. Yumoto, S. Matsuyama, T. Tsumura, H. Okada, T. Masunaga, Y. Senba, Sh. Goto, T. Ishikawa, and K. Yamauchi, "A stitching figure profiler of large X-ray mirrors using RADSI for subaperture data acquisition," Nucl. Instrum. Methods Phys. Res. A **616**(2-3), 229–232 (2010).
23. https://als.lbl.gov/beamlines/8-0-1/
24. http://www.pcgrate.com/about/pcgrates
25. http://henke.lbl.gov/optical_constants/multi2.html BL 6.3.2.

1. Introduction

Diffraction gratings are of great importance for extreme ultra-violet (EUV), soft x-ray, and tender x-ray spectroscopy. They are the heart of soft x-ray monochromators and spectrographs [1–4] utilized at the synchrotrons. Groove placement precision is a key characteristic of x-ray diffraction gratings for high-resolution applications such as Resonant Inelastic X-ray Scattering (RIXS). It is crucial to meet accuracy requirements for groove density distribution for Variable Line Spacing (VLS) gratings which provide focusing and correction of low order aberrations of spectrometer optics.

VLS x-ray gratings are currently produced by diamond burnishing [4,5] or holography techniques [6–8]. Diamond ruling provides grooves of triangular shape optimal for high diffraction efficiency. To achieve high groove placement accuracy tight control of environment conditions is required, which is extremely challenging to maintain over the duration of the ruling process which can be up to a few months for high groove density gratings [9]. Instabilities of any kind in the ruling process result in unwanted variations of the groove density which can affect the resolving power of a spectrometer. Holography is the best way to place every groove in the right position defined by the interference of two waves with ideal wavefronts of a proper shape. This is very challenging though. Any distortions or lack of control of the wavefront shape results in deviation of the local groove density of the interference pattern from the target one. Flexibility in the optical arrangement of a holography system can provide wavefront shape manipulation and allows achievement of an approximation to the required groove density distribution of VLS gratings, precise enough for many x-ray applications. However, the precision requirements are often beyond the manufacturer capabilities and the grating specifications have to be relaxed which affects the design and performance of spectrometers or monochromators. The next generation of ultra-high resolution x-ray instrumentation [3,10,11] requires much higher groove placement accuracy and better groove density distribution control. In this work we suggest an alternative way of making ultra-precise x-ray gratings, which overcomes the traditional grating fabrication techniques. Our approach is based on ultra-precise nanofabrication technologies such as e-beam lithography and large area nanoimprint which provide a nanometer-scale accuracy of groove placement. We demonstrate fabrication of a plane lamellar VLS x-ray grating for use in an x-ray fluorescence spectrometer for RIXS.

2. Fabrication process flow

The nanofabrication-based process for making advanced x-ray gratings is schematically shown in Fig. 1. We use e-beam lithography to record a pattern of any complexity since it provides registration accuracy as high as 1 nm over a large area and a high resolution of writing. After an e-beam resist is exposed the pattern is transferred to a Cr layer sitting on top of a substrate via regular plasma etch. These processes are available commercially. The issue with e-beam lithography is the strict limitations on the shape, dimensions, and material of the substrates. In fact the high accuracy of the e-beam writing is achieved for standard

Optics EXPRESS

semiconductor quartz masks only since the writing process is thoroughly optimized for these particular substrates. Massive and thick x-ray grating blanks of rectangular (and sometimes more complicated) shape are not compatible with commercial e-beam tools. This motivated us to develop a suitable transfer process.

Regular contact UV lithography can be used to transfer an e-beam pattern from the mask to a grating substrate. However, although this would work for gratings with low groove density, up to 300-500 lines/mm, transfer of patterns with a pitch less than a few microns is not possible due to diffraction effects. We developed a transfer process based on large area nanoimprint which can provide replication of grating patterns with groove density up to 10,000 lines/mm. In our process, patterned quartz plates are used for making molds for nanoimprinting (steps #1 and #2 in Fig. 1). An external pressure is applied to the substrate/mold assembly to promote resist flow and filling of the mold grooves. When the nanoimprint resist is cured the mold and the substrate are separated and the residual layer of the imprint is etched with Oxygen plasma (step #3). An adjustment of width of the resist stripes can be done if necessary by use of extended plasma etching. Then rectangular grooves are formed by etching silicon with Fluorine-based plasma (steps #5a and #6a) or alternatively by the lift-off process (steps #5b and #6b) for lamellar gratings.

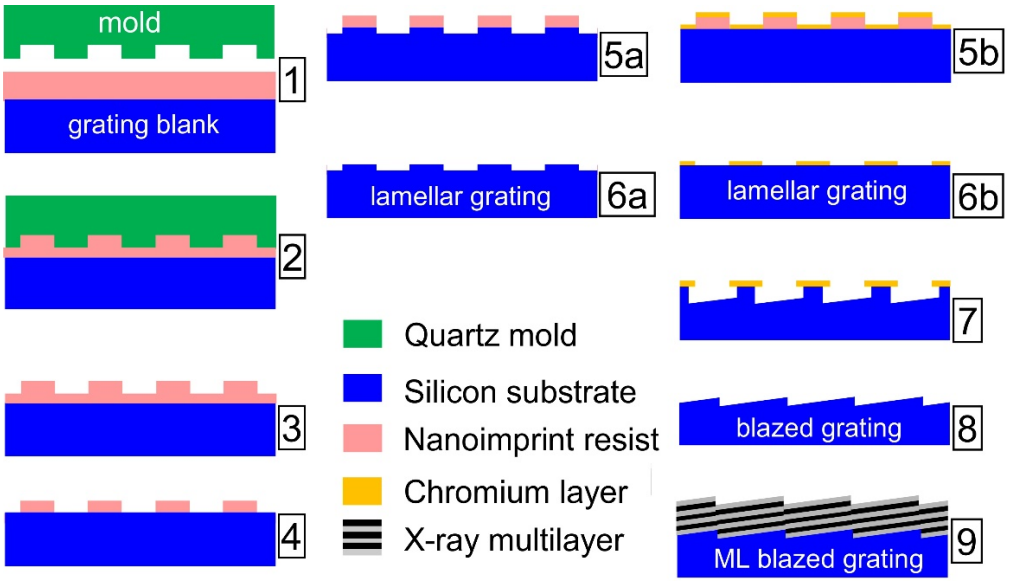

Fig. 1. Schematic representation of a nanofabrication-based process for making advanced x-ray gratings. The process includes large-area nanoimprinting using e-beam patterned molds (steps #1 and #2), plasma etch for residual layer and adjustment of the duty cycle ratio of grating grooves (#3 and #4), silicon dry etch (#5a and #6a) or lift-off process (# 5b and #6b) for lamellar grooves, wet anisotropic etching for blazed grooves (#7 and #8), and multilayer deposition (#9).

A few extra steps are required for making more advanced blazed gratings with slanted facets of the grooves for higher diffraction efficiency. The single crystal Si substrates should have a proper crystallographic orientation. Tilt of the (111) planes of the crystal lattice with respect to the surface of the Si substrate defines the blaze angle of the blazed grating. The Cr stripes obtained by the lift-off process serve as a hard mask for wet anisotropic etching of silicon in alkali solution to obtain slanted facets of the grating grooves (step #7). Alternatively, Silicon Nitride or Silicon Oxide hard masks obtained by plasma etch can be used. Isotropic plasma or wet etching finalize the triangular shape of the grooves of the blazed grating (step #8). The Si gratings are coated with a reflective metal layer for use at grazing incidence or can be coated with a multilayer to enhance diffraction efficiency at substantially

Optics EXPRESS

non-grazing angles, up to normal incidence (step #9). In our previous work we described steps #7-9 in details [12–16]. In this work we focus on the large area nanoimprint step which is a key process for the pattern transfer.

3. Results and discussion

3.1 Nanoimprint and groove placement accuracy

We chose an air cushion press approach for nanoimprinting since it provides high uniformity of pressure distribution over a large area [17]. Nanoimprinting was performed using a UV curable resist mr-UVCur21 along with an adhesion promoter APS-1 from Microresist Technology GmbH [18]. An air cushion imprinting system available at the nanofabrication facility of Molecular Foundry, LBNL [19], capable of accommodating large dimension parts of any shape was used to apply isotropic pressure to the mold/substrate sandwich and to expose the resist.

One needs to make sure that the transfer process preserves high fidelity of e-beam written patterns. To monitor groove density uniformity and groove placement accuracy we used a differential wavefront measurement approach described elsewhere [20,21]. Briefly, a grating is set in the Littrow geometry (when the diffraction angle equals the incidence angle, $\alpha = \beta$) for the 1st "positive" diffraction order in front of a Fizeau phase shifting interferometer and the diffraction wavefront is recorded (Fig. 2). For an ideal constant groove density grating the wavefront is plane while groove density variations result in distortion of the wavefront for the diffracted beam. Displacement, ε, of grating grooves from their ideal positions results in wavefront errors $\sigma = 2\varepsilon \sin\beta$. In this way the wavefront error map reveals irregularities in the grating period of a plane constant groove density grating. Non-planarity of the grating blank surface also contribute to the measured wavefront errors. The contribution is usually negligible for high quality x-ray grating blanks having deviation of 1 - 10 nm peak-to-valley from an ideal plane. On the other hand the surface waviness can be substantial for a medium quality grating blanks or test substrates such as regular semiconductor grade Si wafers, and the surface imperfections can dominate the wavefront errors. To exclude the surface contribution the grating is flipped into the 1st "negative" order diffraction geometry and a second measurements is taken (Fig. 2). Subtraction of the two wavefronts yields differential wavefront errors caused solely by the groove density variations since surface imperfection contribution is the same for both measurements while the groove displacement causes wavefront errors of opposite signs.

VLS gratings have focusing properties and produce substantially curved wavefronts which cannot be measured using the interferometer without additional focusing/collimating optics. The latter however is not desirable since the extra optics would contribute to the total error budget of the measurements. Alternatively, a stitching approach such as relative angle differential stitching interferometry developed for curved x-ray optics measurements [22] could be adopted for the VLS gratings in the future. In this work we used a test constant groove density grating to characterize our pattern transfer process in terms of groove placement accuracy. We chose a high groove density of 2000 lines/mm for the test grating to increase sensitivity of the wavefront measurements (since wavefront errors are related to the groove displacement via the Littrow angle, the sensitivity of the wavefront measurements increases with the groove density).

An e-beam grating pattern with dimensions of 120 mm × 30 mm that was transferred to a 70 nm thick Cr layer on a 6" × 6" × 1/4" quartz plate (Fig. 3(a)) was obtained commercially. A CHF_3 / O_2 plasma was used to etch 350 nm deep grooves in the quartz and then the Cr layer was stripped off by a regular Cr etchant. The fabricated negative-profile mold was coated with an anti-sticking coating (1H,1H,2H,2H-Perfluorooctyltriethoxysilane).

The test pattern was replicated on a semiconductor prime grade 6" Si wafer. The wafer was spin-coated with the adhesion promoter layer which was baked at 150°C and then spin-coated with the nanoimprint resist. The wafer and the mold were pressed together and the

Optics EXPRESS

mold/wafer sandwich was put between two UV-transparent membranes. Then an external pressure of 90 psi was applied via a cushion press and the resist was exposed with UV light through the transparent quartz mold to cure the resist.

After mold/substrate separation, the Si wafer was inspected for imprint imperfections. A few particle contamination defects were observed on the imprint (Fig. 3(b)). It is crucial to eliminate any particle defects for real x-ray gratings but they can be tolerated for this test pattern since they located out of the pattern area. The imprint exhibits a lot of interference fringes which indicates some non-uniformity of the resist layer thickness. The non-uniformity is caused by the particle defects mostly, but the fringes observed within the patterned area are probably caused by redistribution of the resist and its penetration into the mold grooves and bending of the thin Si wafer under the external pressure applied.

The residual layer was etched through by use of Oxygen plasma and then a 20 nm thick Cr layer was deposited. Piranha solution was used to remove the resist leaving the pattern consisting of Cr stripes on Si surface (Fig. 3(c)).

Wavefront measurements were performed for both the mold and the transferred pattern. The e-beam written pattern of the mold exhibits extremely low wavefront errors confirming very high groove density uniformity over the whole area of the test grating (Fig. 4(a)). At the same time the imprinted pattern has some non-uniformity of the wavefront map (Fig. 4(b)). This indicates that superior quality of the e-beam pattern has somewhat degraded and the groove placement errors introduced by the transfer process increased by a factor of 3 from +/– 5 nm to +/– 15 nm p/v for the mold and the imprint respectively. Nevertheless, the groove placement errors are still very small. In our experience, x-ray gratings recorded by the holographic approach typically have at least an order of magnitude higher groove placement errors. A groove placement errors of +/– 15 nm (Fig. 4(d)) results in negligible variations of 0.002 lines/mm rms of groove density of the grating (Fig. 4(e)). We can conclude that the high accuracy of the e-beam written patterns is mostly preserved by the large area nanoimprint transfer process, at the level of accuracy required.

There is some similarity between the wavefront error map and the fringe pattern observed for the imprint (compare images in Fig. 4(b) and Fig. 3(b)) which indicates that the groove placement errors are possibly related to the resist layer thickness non-uniformity. If, in turn, the thickness non-uniformity is caused by flexibility of the thin wafer one can expect higher thickness uniformity and hence smaller groove placement errors for a thick non-flexible substrate.

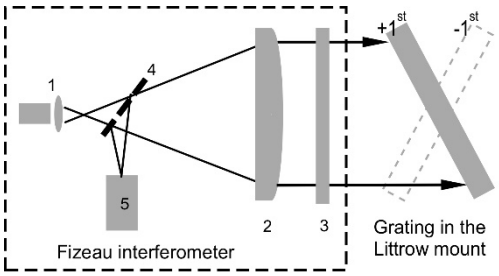

Fig. 2. Schematic arrangement of the wavefront measurements for groove placement accuracy monitoring. A diffraction grating is mounted in the Littrow configuration in front of a Fizeau phase shifting interferometer (1 - laser, 2 – collimator, 3 – reference flat, 4- beam splitter, 5 – camera). Two wavefronts for positive and negative order diffraction geometry are recorded. Difference between the wavefronts exhibits an error map caused by displacement of grating grooves from their ideal positions.

Optics EXPRESS

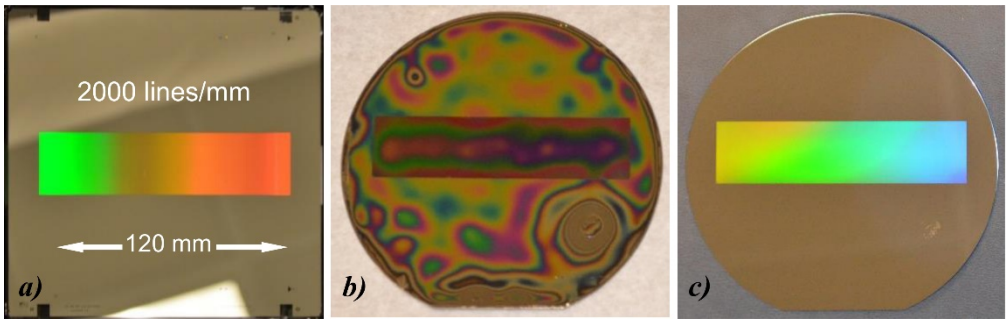

Fig. 3. Photographs of 120 × 30 mm^2 2000 lines/mm test grating: e-beam written Cr pattern on 6" × 6" × 1/4" quartz plate mold (a), the pattern transferred to the nanoimprint resist on a 6" semiconductor Si wafer (b), Cr pattern on the Si wafer transferred by lift-off (c).

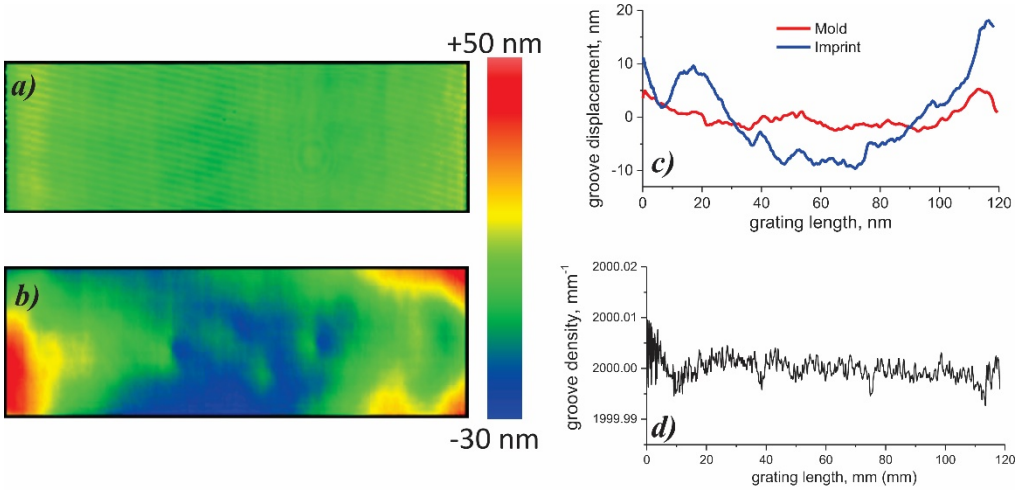

Fig. 4. Differential wavefront error maps for the mold (a) and imprint (b) of the 2000 lines/mm test pattern (full color scale corresponds to peak-to-valley wavefront errors of +/–40 nm for the both maps); average profiles of the error maps (c); groove density of the imprinted pattern calculated in terms of the wavefront errors (d).

3.2 Fabrication of a VLS lamellar grating for a soft x-ray spectrometer

As a demonstration, we applied the nanofabrication-based approach to produce a lamellar grating for a soft x-ray RIXS spectrometer at the beamline 8.0.1 at the Advanced Light Source synchrotron x-ray radiation facility [23]. The Hettrick-Underwood design [1] of the spectrometer requires a VLS grating with a groove density $g = g_0 + g_1 w + g_2 w^2 + g_3 w^3$, where w is a coordinate along the grating length, and the polynomial coefficients are: g_0 = 900 mm^{-1}, g_1 = 1.29154 mm^{-2}, g_2 = 8.84197 × 10^{-4} mm^{-3}, g_3 = 3.62557 × 10^{-7} mm^{-4}. Since the groove density in the center of the VLS grating is 900 lines/mm, in the following we will refer to the grating as the 900 lines/mm VLS grating.

The parameters of the grating grooves such as the duty cycle ratio and groove depth were optimized to achieve the highest possible efficiency for the central energy of 600 eV of the operational energy range of 440-880 eV. Calculations of the diffraction efficiency for a wide range of groove parameters were performed using a code based on the integral formalism of the electromagnetic theory of grating diffraction [24]. Figure 5 shows the dependence of the efficiency for a particular groove depth for different duty cycle ratios. An optimal groove depth of 10.8 nm and a duty cycle ratio is 0.3 provide the highest diffraction efficiency. Substantial deviation of the groove parameters from the ideal ones would result in significant reduction of the diffraction efficiency. On the other hand realistic fabrication tolerances of

Optics EXPRESS

+/– 1 nm for the groove depth and +/–0.05 for the duty cycle are not expected to harm the diffraction efficiency dramatically.

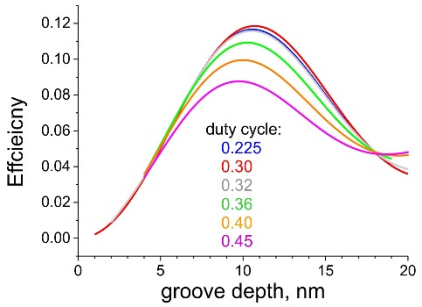

Fig. 5. Dependence of theoretical diffraction efficiency of a 900 lines/mm grating on a groove depth for different duty cycle ratios at the energy of 600 eV and the incidence angle of 88.854°.

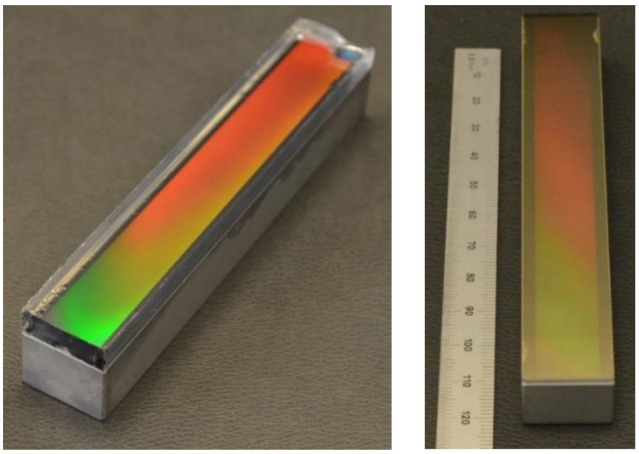

Fig. 6. Grating substrate/quartz mold sandwich exhibits defect free large area imprinting (left). Final 900 lines/mm lamellar VLS grating coated with a gold layer (right).

The mold for the VLS grating was fabricated similar to the one for the test grating (see paragraph 3.1). After the plasma etch, the quartz plate was diced down to the dimensions of 120 mm × 20 mm to match the dimensions of the 15 mm thick silicon substrate of the grating. A photograph of the mold/substrate sandwich after the UV cure step is shown in Fig. 6(a). Inspection of the pattern reveals no particle contamination defects and a high uniformity of the resist layer thickness.

A duty cycle ratio of 0.5 of the imprinted resist patterns corresponds to the design of the mold grooves (Fig. 7(a)). In our experience the ratio of 0.5 is most optimal for the nanoimprint since it provides the lowest possible aspect ratio for both mold and imprint features. The low aspect ratio (i.e. the ratio of feature height to the feature width) is favorable to reduce the risk of damage of the resist patterns during mold/substrate sandwich separation and especially important for thick non-flexible molds and substrates. On the other hand the duty cycle ratio of 0.5 is not optimal for high diffraction efficiency (see Fig. 5) and should be modified. After the residual layer etch with Oxygen plasma some extra etching was applied to the resist pattern until the optimal duty cycle of 0.3 was achieved (Fig. 7(b)). Parameters of the Oxygen plasma were optimized to reduce anisotropy of the etching to provide etching the sidewalls of the resist stripes and reduce their width. A following step of CHF_3 etching transferred the pattern into the silicon substrate. Some increase of the duty cycle ratio was observed for that step (Fig. 7(c)) resulting in a final duty cycle ratio of 0.33 which is within

Optics EXPRESS

the tolerances. A photograph and an AFM image of the finalized grating coated with a reflective Au layer are shown in Figs. 6(b) and 8 respectively.

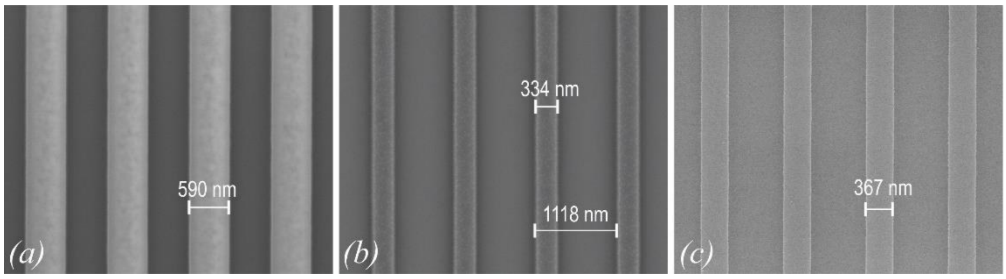

Fig. 7. SEM images of the 2000 lines/mm resist pattern after nanoimprint (a), after duty cycle adjustment by Oxygen plasma etch (b), and the final Si grating after CHF_3 plasma etch and resist removal (c).

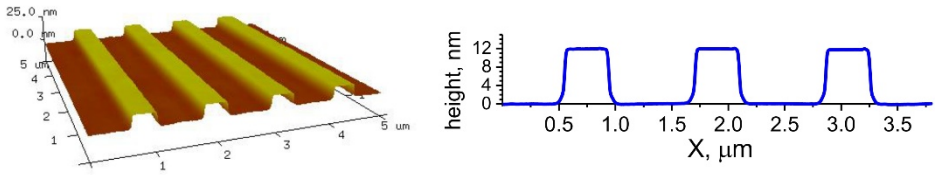

Fig. 8. An AFM image and a groove profile of the 900 lines/mm VLS grating.

Diffraction efficiency measurements of the 900 lines/mm lamellar grating were performed at beamline 6.3.2 [25] of the ALS by detector angle scanning at an incidence angle of 88.85° from the grating normal in the 400-900 eV energy range. One of the detector scans for an energy of 600 eV is shown in Fig. 9(a). The measured diffraction efficiency of 11% corresponds closely to the theoretical value (red curve in Fig. 9) calculated for the experimentally measured duty cycle ratio of 0.33 (see Fig. 7(c)) and the groove depth of 11.7 nm (see the AFM profile in Fig. 8). Although both the groove depth and the duty cycle of the fabricated grating are within the excepted tolerances, the efficiency simulations (Fig. 9(b)) show that the efficiency can be slightly improved provided tighter tolerances for the groove depth and the duty cycle are achieved.

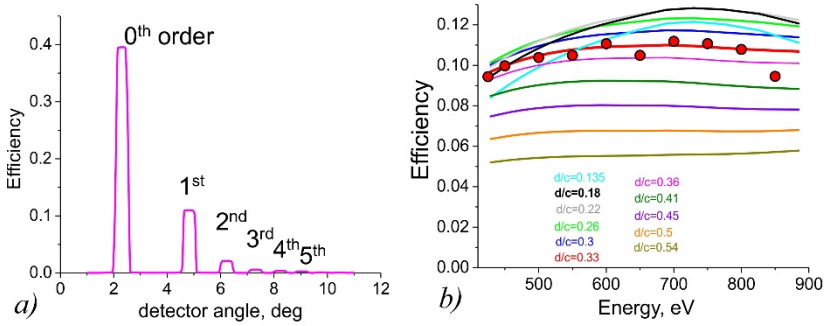

Fig. 9. Detector angle scan for the incidence angle of 88.85° and an energy of 600 eV (a). Efficiency of the 1st diffraction order in a wide energy range (b): experimental efficiency is shown with symbols; theoretical efficiency calculated for the AFM measured groove depth of 11.7 nm and different duty cycle ratios are shown with the curves.

Summary

We developed a new process for fabrication of ultra-precise x-ray diffraction gratings for advanced spectroscopic applications. The process is based on a set of nanofabrication techniques which were adapted for making large dimension x-ray gratings. Grating patterns

Optics EXPRESS

are recorded by e-beam lithography which provides nanometer scale accuracy for groove placement, and then transferred to a massive grating blank using large area nanoimprint followed by plasma etching. The transfer process does not introduce appreciable groove density errors and provides preservation of the high groove placement accuracy. The fabricated 900 lines/mm lamellar VLS grating demonstrated diffraction efficiency close to the theoretical value. The fabrication process allows the manufacture of diffraction gratings of any groove density including ultra-high density gratings with very high fidelity and with any degree of complexity of the groove density variation. This opens up new possibilities for the design of ultra-high resolution x-ray spectrometers. It should be noted that the nano-imprint molds can be reused, significantly reducing the fabrication time and cost for multiple gratings.

Acknowledgments

Advanced Light Source and Molecular Foundry are supported by the Director, Office of Science, Office of Basic Energy Sciences, of the U.S. Department of Energy under Contract No. DE-AC02-05CH11231.

Disclaimer

This document was prepared as an account of work sponsored by the United States Government. While this document is believed to contain correct information, neither the United States Government nor any agency thereof, nor The Regents of the University of California, nor any of their employees, makes any warranty, express or implied, or assumes any legal responsibility for the accuracy, completeness, or usefulness of any information, apparatus, product, or process disclosed, or represents that its use would not infringe privately owned rights. Reference herein to any specific commercial product, process, or service by its trade name, trademark, manufacturer, or otherwise, does not necessarily constitute or imply its endorsement, recommendation, or favoring by the United States Government or any agency thereof, or The Regents of the University of California. The views and opinions of authors expressed herein do not necessarily state or reflect those of the United States Government or any agency thereof or The Regents of the University of California.